Biochimica et Biophysica Acta 1840 (2014) 1634–1639

Contents lists available at ScienceDirect

Biochimica et Biophysica Acta

journal homepage: www.elsevier.com/locate/bbagen

Validation of NCM460 cell model as control in antitumor strategies targeting colon adenocarcinoma metabolic reprogramming: Trichostatin A as a case study

Gema Alcarraz-Vizán [a,1], Susana Sánchez-Tena [a], Mary Pat Moyer [b], Marta Cascante [a,*]

[a] Department of Biochemistry and Molecular Biology, IBUB, Faculty of Biology, Universitat de Barcelona and Unit Associated with CSIC, 08028 Barcelona, Spain
[b] INCELL Corporation, San Antonio, TX 78249, USA

ARTICLE INFO

Article history:
Received 18 July 2013
Received in revised form 18 November 2013
Accepted 17 December 2013
Available online 22 December 2013

Keywords:
Colon cancer
Glycolysis
Metabolic adaptation
Metabolic profile
Tumour metabolism
Trichostatin-A

ABSTRACT

Background: Cancer cells have extremely active metabolism, which supports high proliferation rates. Metabolic profiles of human colon cancer cells have been extensively studied, but comparison with non-tumour counterparts has been neglected.
Methods: Here we compared the metabolic flux redistribution in human colon adenocarcinoma cells (HT29) and the human colon healthy cell line NCM460 in order to identify the main pathways involved in metabolic reprogramming. Moreover, we explore if induction of differentiation in HT29 by trichostatin A (TSA) reverts the metabolic reprogramming to that of NCM460. Cells were incubated with [1,2-$^{13}C_2$]-D-glucose as a tracer, and Mass Isotopomer Distribution Analysis was applied to characterize the changes in the metabolic flux distribution profile of the central carbon metabolism.
Results: We demonstrate that glycolytic rate and pentose phosphate synthesis are 25% lower in NCM460 with respect to HT29 cells. In contrast, Krebs cycle activity in the former was twice that recorded in the latter. Moreover, we show that TSA-induced HT29 cell differentiation reverts the metabolic phenotype to that of healthy NCM460 cells whereas TSA does not affect the metabolism of NCM460 cells.
Conclusions: We conclude that pentose phosphate pathway, glycolysis, and Krebs cycle are key players of colon adenocarcinoma cellular metabolic remodeling and that NCM460 is an appropriate model to evaluate the results of new therapeutic strategies aiming to selectively target metabolic reprogramming.
General significance: Our findings suggest that strategies to counteract robust metabolic adaptation in cancer cells might open up new avenues to design multiple hit and targeted therapies.

1. Introduction

Metabolic adaptation in cancer has attracted the attention of the scientific community in recent years because of its simultaneous robustness and fragility. In this regard, metabolomics can map the metabolic adaptation made by cancer cells to cover the demands for metabolite building blocks and energy to support sustained high proliferation rates. This adaptation includes, among others, the Warburg effect (high glycolysis in the presence of oxygen) [1], high glutamine uptake, activation of biosynthetic pathways, and overexpression of some glycolytic isozymes [2]. These robust characteristics confer advantages for cancer cell proliferation but can also be an Achilles' heel in this disease because the deep metabolic flux redistribution required to support these metabolic demands induces changes in the normal metabolic homeostasis of the cell, thus making the cancer cell more sensitive to unexpected perturbations via drugs that target metabolism [3]. However, few studies have characterized or compared the metabolic flux distribution through the glucose central metabolic network of tumour and non-tumour cell counterparts.

In this regard, detailed knowledge of the metabolic adaptation of cancer cells and how adaptation differs from healthy cells could contribute to the development of multiple-hit therapies that target individual enhanced metabolic fluxes and the whole network of cancer cells. Techniques that allow the monitoring not only of the changes in metabolite levels but also metabolic fluxes, in particular tracer-based metabolomics, are essential to characterize the state of the metabolic network. Fluxomics, a discipline derived from metabolomics, provides a more detailed footprint than that represented by the phenotype. For this purpose, ^{13}C-labelled glucose allows the study of the glucose metabolic network, including glycolysis, the Krebs cycle and the pentose phosphate pathway (PPP) [4]. It also contributes to determining how differences in glucose uptake correlate with fluxes through the various metabolic pathways. Changes in tumour metabolism should be viewed not only as the consequences of other cellular mechanisms or the

* Corresponding author at: Department of Biochemistry and Molecular Biology, Universitat de Barcelona, Faculty of Biology (Prevosti Building), Av. Diagonal 643, 08028 Barcelona, Spain. Tel.: +34 934021593.
E-mail address: martacascante@ub.edu (M. Cascante).
[1] Current address: Diabetes and Obesity Laboratory, Institut d'Investigacions Biomèdiques August Pi i Sunyer (IDIBAPS), Centre Esther Koplowitz (CEK), 08036 Barcelona, Spain.

0304-4165/$ – see front matter © 2013 Elsevier B.V. All rights reserved.
http://dx.doi.org/10.1016/j.bbagen.2013.12.024

endpoint of several signalling cascades. Increasing evidence shows bidirectional crosstalk between metabolic and genetic alterations and also metabolic changes that trigger transcriptional and epigenetic alterations that drive cell fate. In this framework, the reversion of the metabolic phenotype of the cancer cell to that of a healthy cell may offer a promising strategy for cancer treatment.

According to the World Health Organization, colon cancer is the fourth leading cause of cancer deaths worldwide. Many studies performed predominantly with human colon cancer cells show the Warburg effect. Cell lines that are suitable models of healthy human colon cells, such as the NCM460 line [5], have recently become available; however, the metabolic flux distribution on these cells has not been characterized to date.

Here we characterized the metabolic profile of NCM460 cells, a cell line derived from healthy mucosal epithelium from the human colon. Using [1,2-$^{13}C_2$]-D-glucose and Mass Isotopomer Distribution Analysis (MIDA), we compared this non-tumour cell line with the human colon adenocarcinoma cell line HT29. We demonstrate that NCM460 cells differ metabolically from tumour cells regarding the glycolytic pathway, ribose synthesis, and Krebs cycle utilization. Furthermore, we used the well-known histone deacetylase inhibitor trichostatin-A (TSA) [6] to induce cell differentiation in HT29 cells and to check whether differentiation-induced metabolic changes correlate with a reversion of the tumour metabolic phenotype to that of NCM460 cells.

Our results contribute to a better understanding of the differences between the glucose metabolic network in healthy and cancer cells. Moreover, demonstration that TSA reverts the tumour phenotype will help guide researchers towards a rational design of multiple hit therapies targeting the pathological state of the metabolic network in cancer cells while simultaneously minimizing the effects on healthy ones.

2. Materials and methods

2.1. Chemicals

All chemicals were purchased from Sigma–Aldrich Co (St Louis, MO, USA), unless otherwise specified. Dulbecco's Modified Eagle's Medium (DMEM) and antibiotic (10,000 U/mL penicillin, 10,000 μg/mL streptomycin) were obtained from Gibco-BRL (Eggenstein, Germany), foetal calf serum (FCS) was purchased from PAA Laboratories (Pasching, Austria) and trypsin-EDTA solution C (0.05% trypsin-0.02% EDTA) from Invitrogen (Paisley, UK). Stable [1,2-$^{13}C_2$]-D-glucose isotope was obtained with >99% purity and 99% isotope enrichment for each position from Isotec Inc. (Miamisburg, OH). M3Base medium was purchased from INCELL (Texas, US).

2.2. Cell culture

Human colorectal adenocarcinoma HT29 cells (American Type Culture Collection, HTB-38) were grown as a monolayer culture in DMEM with 4 mM L-glutamine, without glucose and without sodium pyruvate, in the presence of 10% heat-inactivated FCS, 10 mM of D-glucose and 0.1% streptomycin/penicillin in standard culture conditions. NCM460, obtained through a Material Transfer Agreement with INCELL, is an epithelial cell line derived from the healthy colon mucosa of a 68-year-old Hispanic male [7]. These cells were grown as a monolayer culture in M3Base medium (which contains growth supplements and antibiotics) supplemented with 10% heat-inactivated FCS and 2.5 mM of D-glucose (final concentration 5 mM glucose, 2 mM glutamine). Cell cultures were carried out at 37 °C in a 95% air, 5% CO_2, humidified environment.

Due to the different growing of the cell lines HT29 and NCM460 cell cultures were started with 3×10^5 and 1×10^6 cells respectively, which were achieved using standard cell counting techniques. 72 h (HT29) and 24 h (NCM460) after seeding, cell medium was removed and fresh medium supplemented with [1,2-$^{13}C_2$]-D-glucose (50% isotope enrichment) was added with or without 180 nM TSA, which corresponds to the IC_{50} value of TSA on HT29 cell viability [8]. The viability of NCM460 cells at this TSA concentration was 85%. The cells were harvested 72 h after treatment.

2.3. Glucose and lactate

The concentrations of glucose and lactate in cell medium were measured spectrophotometrically. Glucose was measured using a Cobas Mira chemistry analyzer (Roche Applied Science) and lactate using an ELISA plate reader (Tecan Sunrise MR20-301, TECAN).

To measure lactate by GC/MS, this metabolite was extracted as described elsewhere [9]. The m/z 328 (carbon atoms 1–3 of lactate, CI) was monitored for the detection of m0 (unlabelled species), m1 (lactate with one ^{13}C atom) and m2 (lactate with two ^{13}C atoms) [9]. Glycolytic rate was calculated as $m2_{lactate}/(m2_{glucose}/2)$. Lactate enrichment was calculated as $\sum mn = m1 + m2 \times 2 + m3 \times 3$.

2.4. RNA ribose

Ribose was isolated from RNA and derivatized to its aldonitrile acetate as previously described [9]. The ion cluster around the m/z 256 (carbon atoms 1–5 of ribose, CI) was monitored. The oxidative *versus* non-oxidative ratio was measured as $ox/non\text{-}ox = (m1 + m3)/(m2 + m3 + 2 \times m4)$, since m1 and m3 require the formation of the oxidative branch, whereas m2, m3 and m4 species require the non-oxidative one (twice in m4). Ribose enrichment was calculated as $\sum mn = m1 + m2 \times 2 + m3 \times 3 + m4 \times 4 + m5 \times 5$.

2.5. Glutamate

Glutamate was separated from the cell medium as described elsewhere [10]. Glutamate was converted to its n-trifluoroacetyl-n-butyl derivative and the ion cluster m/z 198 (carbon atoms 2–5, C2–C5, of glutamate, EI) was monitored. Glutamate enrichment was calculated as $\sum mn = m1 + m2 \times 2 + m3 \times 3 + m4 \times 4$ from the C2–C5 glutamate fragment.

Glutamate and glutamine concentrations in the culture medium were measured spectrophotometrically using a Cobas Mira chemistry analyzer (Roche Applied Science).

2.6. Gas chromatography/mass spectrometry

Mass spectral data were obtained on a GCMS-QP2010 selective detector connected to a GC-2010 gas chromatograph from Shimadzu. The settings were as follows: GC inlet 250 °C (200 °C for lactate measurement), transfer line 280 °C, MS Quad 150 °C. A DB-5MS capillary column (30 m length, 250 μm diameter and 0.25 μm film thickness) was used for the analysis of ribose, glutamate and lactate.

2.7. Data analysis and statistical methods

In vitro experiments were carried out using three cultures each time for each treatment and then repeated three times. Mass spectral analyses were performed by three independent injections of 1 μL of each sample by the automatic sampler and were accepted only when the standard sample deviation was less than 1% of the normalized peak intensity. Statistical analyses were performed using the parametric unpaired, two-tailed independent sample *t* test with 99% confidence intervals. $p < 0.01$ (*) was considered to indicate significant differences in glucose carbon metabolism in HT29 and NCM460 cell cultures treated with TSA and between HT29 and NCM460 control cells.

3. Results

3.1. Differences in glucose consumption and lactate production between NCM460 and HT29 cells

Glucose consumption and lactate production were measured in NCM460 and HT29 cells before and after TSA treatment. Non-treated NCM460 cells consumed approximately 50% less glucose than non-treated HT29 cells and lactate production was also lower for the former (Fig. 1A). In contrast, TSA treatment reduced glucose consumption and lactate production in HT29 cells but not in NCM460. As a result, when treated with TSA, the HT29 cells showed a similar glycolytic profile to that of the NCM460 line (HT29 results from [8]).

3.2. Differences in glycolytic flux between NCM460 and HT29 cells

Lactate is secreted into the cell medium and provides useful information about the contribution of glycolysis and the PPP to the central glucose metabolism. When [1,2-$^{13}C_2$]-D-glucose is metabolized by glycolysis, m2 lactate is produced, whereas flux of labelled glucose through the oxidative and non-oxidative branches of the PPP results in m1 lactate [11]. Table 1 shows the isotopomeric distribution of lactate for NCM460 and HT29 cells with or without TSA treatment. NCM460 control cells presented a higher m0 value than untreated HT29 cells, thus indicating less lactate formation from glucose, which was corroborated by less total ^{13}C lactate enrichment (Fig. 1B) (HT29 results from [8]), calculated as described in the *Material and Methods* section. Consequently, the glycolytic rate (Fig. 1C) (HT29 results from [8]), estimated as $m2_{lactate}$ divided by $m2_{glucose}/2$ ($m2_{glucose}$ being 48.99 %, data not shown), was over 80 % for HT29 cells and only approximately 60 % for NCM460 ones. Regarding TSA treatment, it reduced the m2 lactate value in both cell lines, but the m0 value increased only in HT29 cells, thereby indicating that the biological relevance was significant only in this cell line (Table 1). Moreover, the capacity of TSA to reduce ^{13}C lactate enrichment was observed only in cancer cells, thus making HT29 metabolism more similar to that of the untreated NCM460 cells (Fig. 1B). TSA treatment also decreased the glycolytic rate in both cell lines; however, of note, the effect was much more pronounced in HT29 cells (Fig. 1C).

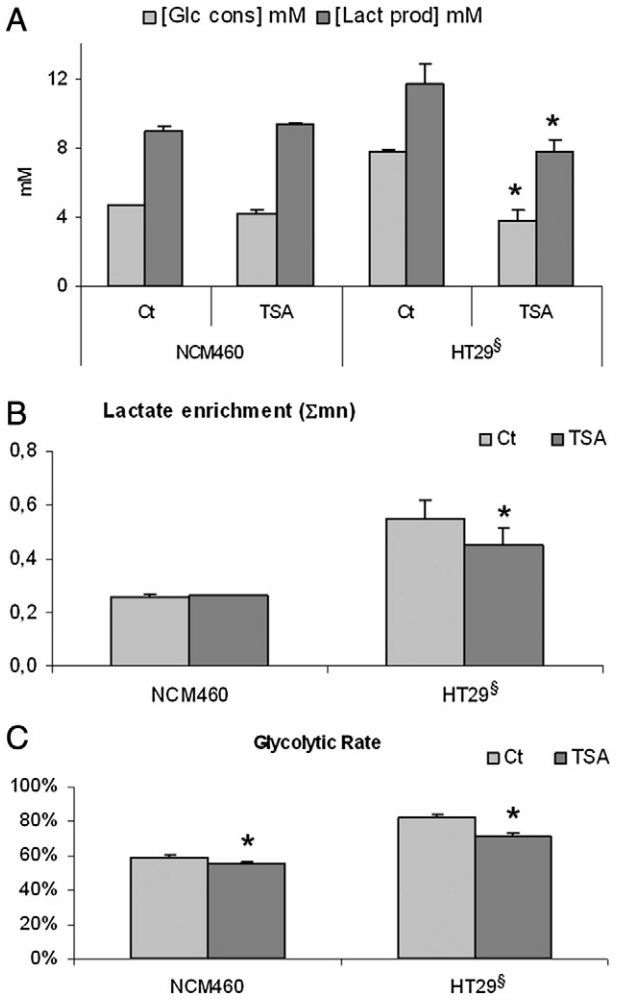

Fig. 1. A, Glucose consumption and lactate production of NCM460 and HT29 cells before and after TSA treatment. **B**, Total ^{13}C lactate molar enrichment from labelled glucose was calculated as $\sum_{mn} = m1 + 2 \times m2 + 3 \times m3$ in NCM460 and HT29 cells before and after treatment. **C**, Glycolytic rate of NCM460 and HT29 in response to TSA treatment expressed as $m2_{lactate}/(m2_{glucose}/2)$. Ct, control cells; TSA, trichostatin-A treated cells. $p < 0.01$ (*) was considered to indicate statistic significant differences between TSA-treated and non-treated cells in each cell line. § HT29 results from [8].

Table 1
Lactate isotopomer distribution in NCM460 and HT29 cells after TSA treatment. Ct, control cells; TSA, trichostatin-A-treated cells. $p < 0.01$ (*) was considered to indicate statistic significant differences between TSA-treated cells and non-treated cells in each cell line.

LACTATE	m0	m1	m2	LACTATE	m0	m1	m2
NCM460	83.66%	2.55%	14.40%	HT29	71.52%	3.45%	19.69%
Ct	0.51%	0.39%	0.42%	Ct	2.49%	0.75%	0.22%
NCM460	83.74%	2.62%	13.57%*	HT29	75.08%*	2.70%	19.00%*
TSA	0.12%	0.06%	0.12%	TSA	2.75%	1.08%	0.36%

3.3. NCM460 cells exhibit an active tricarboxylic acid cycle

We studied the tricarboxylic acid (TCA) cycle following two approaches. First, glutamate and glutamine concentrations were measured in the two cell lines to determine glutamine uptake and glutamate production. In HT29 cells glutamine consumption was twice that in NCM460 cells (Fig. 2A). Treatment of HT29 cells with TSA reduced this parameter to values similar to those of control NCM460 cells. TSA treatment did not change glutamine consumption significantly in NCM460 cells. Regarding glutamate production, HT29 produced more glutamate than NCM460 cells and TSA reduced this parameter only in the tumour cell line (Fig. 2A).

Furthermore, measurement of ^{13}C label in glutamate reflects the utilization of the TCA cycle, both with regard to glucose metabolization and glutamine uptake. The more glucose is oxidized through the mitochondrial respiratory chain, the more label in glutamate that will be detected; in contrast, the more glutamine is consumed from the media, the less fraction of label will be present in glutamate as a result of carbon dilution of the label. Analysis of total glutamate isotopomer distribution showed greater label incorporation in the healthy NCM460 cells in the C2–C5 glutamate fragment (Table 2). This observation indicates a major contribution of glucose carbon atoms to the Krebs cycle.

Moreover, total ^{13}C glutamate enrichment was higher in non-tumour cells (0.287 for NCM460 *vs.* 0.128 for HT29 cells) (as can be seen in Fig. 2B and Table 2). In this case, TSA significantly reduced glutamate enrichment in both cell lines.

3.4. NCM460 and HT29 cells make different uses of the Pentose Phosphate Pathway

Due to the characteristics of the PPP, label incorporation into ribose shows m1 and m2 as major isotopomers, but m3 and m4 species are also formed. The results from the isotopomer distribution showed that NCM460 cells incorporated less ^{13}C into RNA ribose (Table 3 and Fig. 2C) than HT29 cells, agreeing with a higher nucleotide synthesis rate in the latter. TSA enhanced the total ^{13}C ribose enrichment in NCM460 cells (Fig. 2C). In contrast, TSA treatment reduced total ^{13}C ribose enrichment in HT29 cells (Fig. 2C).

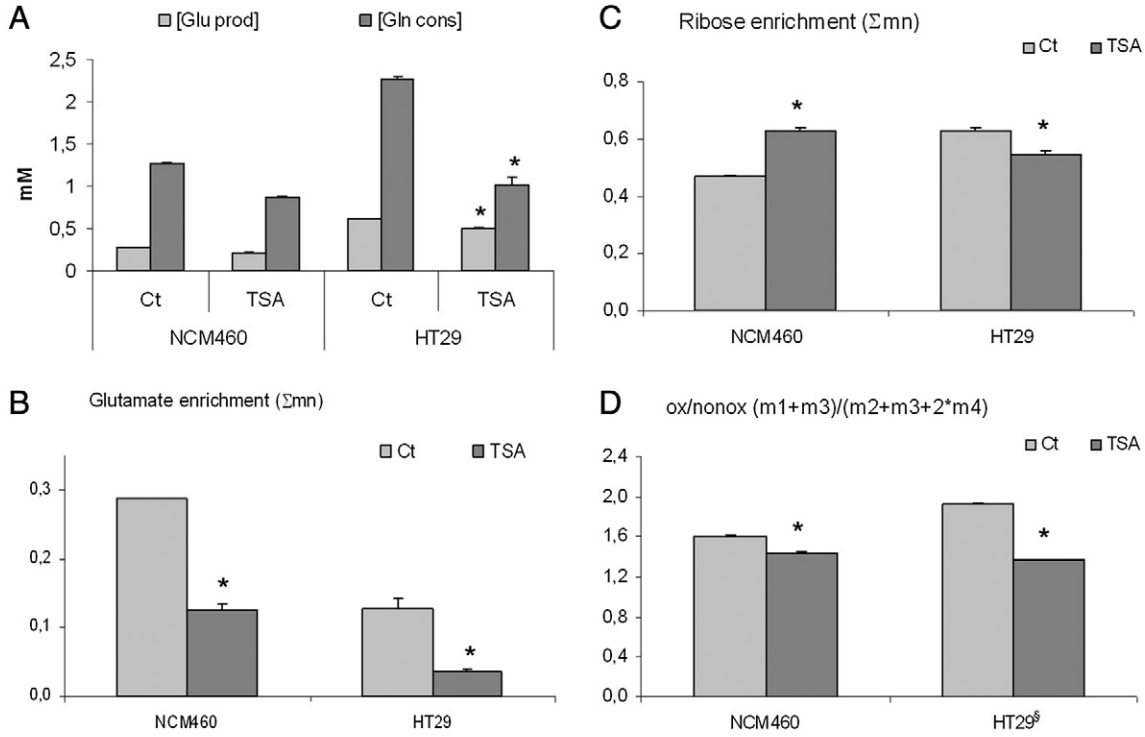

Fig. 2. A, Determination of glutamate production and glutamine consumption of NCM460 and HT29 cells after TSA treatment. **B**, Total ^{13}C glutamate molar enrichment in NCM460 and HT29 cells treated with TSA. Enrichment was calculated as $\sum_{mn} = m1 + 2 \times m2 + 3 \times m3 + m4 \times 4$ from the C2–C5 glutamate fragment. **C**, Total ^{13}C RNA ribose molar enrichment in NCM460 and HT29 cells treated with TSA. Enrichment was calculated as $\sum_{mn} = m1 + 2 \times m2 + 3 \times m3 + m4 \times 4 + m5 \times 5$. **D**, The contribution of oxidative *vs.* non-oxidative branches of the PPP was calculated from the isotopomeric distribution of RNA ribose as ox/non-ox $= (m1 + m3)/(m2 + m3 + 2 \times m4)$. Ct, control cells; TSA, trichostatin-A treated cells. $p < 0.01$ (*) was considered to indicate statistic significant differences between TSA-treated cells and non-treated cells in each cell line. § HT29 results from [8].

Fig. 2D shows the ratio between fluxes through the oxidative and non-oxidative branches of the PPP estimated using the data in Table 3 following the formula ox/non-ox $= (m1 + m3)/(m2 + m3 + 2 \times m4)$. The ox/non-ox ratio in NCM460 cells was lower than in HT29 ones (Fig. 2D). These observations indicate that tumour cells not only have an enhanced PPP when compared to their non-tumour counterparts but also a higher dependence on the oxidative pathway of the PPP. Moreover, TSA treatment reduced this ratio by 30% in tumour cells and by only 10% in the non-tumour cell line (HT29 results from [8]).

4. Discussion

The tumour metabolome describes the characteristic metabolic phenotype of cancer cells. Several common features of the tumour metabolome have been described, such as high glucose and glutamine consumption and an increase in the gene expression of glycolytic enzymes triggered by a number of oncogens. However, enhanced glucose consumption can be rerouted through distinct metabolic pathways; for example, NIH-3 T3 cells transfected with different *K-ras* mutations show alternative metabolic fingerprints [12]. Therefore, a better knowledge of the tumour metabolic profile will allow the rational design of specific therapies in concordance with the precise tumour adaptation.

Our results, summarized in Fig. 3, demonstrate that non-cancer NCM460 human colon cells exhibit a metabolic profile that differs from that of HT29 human colon adenocarcinoma cells. In addition, we show that the differentiation inducer TSA reverts the tumour metabolic profile of HT29 cells. In particular, NCM460 cells consumed 40% less glucose and produced 25% less lactate than their tumour counterparts. This decrease was also observed in the glycolytic rate and in lactate enrichment, which were also lower for non-tumour cells. All these results are consistent with the Warburg effect observed in tumour cells. Glucose and glutamine are crucial substrates in tumour cells because they provide energy and carbon material to assure high proliferation rates. Glutamine uptake is normally enhanced in cancer cells while inhibition of glutaminolysis decreases tumour cell proliferation [13]. Our results show that NCM460 cells exhibited a lower glutamine uptake than the cancer cell line HT29. This finding is consistent with its non-tumour phenotype. In addition, it has been widely described that tumour cells preferentially use glycolysis to obtain energy rather than the Krebs, or tricarboxylic acid (TCA), cycle [14]. In this regard, NCM460 cells showed a more active TCA cycle, as shown by enhanced total glutamate ^{13}C enrichment.

Interestingly, the PPP is down-regulated during cell differentiation [10]; however, activation of this pathway is a common characteristic of tumour cells [15,16]. The PPP can be separated into two branches, one oxidative and one non-oxidative. A high ox/non-ox ratio is a characteristic of colon tumours and a decrease in the ratio by a multiple-hit drug strategy results in colon adenocarcinoma cell death [16,17]. Here we show that NCM460 cells exhibit a lower ox/non-ox ratio and total ribose ^{13}C enrichment than HT29 cells. This finding corroborates that the non-cancer cell line and its cancer counterpart have distinctive metabolic profiles.

Table 2
Glutamate isotopomer distribution of ^{13}C, expressed as % of total glutamate, in NCM460 and HT29 cells before and after treatment with TSA. Ct, control cells; TSA, trichostatin-A-treated cells. $p < 0.01$ (*) was considered to indicate statistic significant differences between TSA-treated cells and non-treated cells in each cell line.

C2–C5	m0	m1	m2	m3	m4
NCM460	82.39%	7.84%	8.68%	0.87%	0.22%
Ct	0.04%	0.02%	0.02%	0.01%	0.01%
NCM460	92.15%*	3.36%*	4.30%*	0.15%*	0.03%*
TSA	0.51%	0.24%	0.19%	0.08%	0.05%
HT29	92.72%	2.53%	4.22%	0.32%	0.21%
Ct	0.86%	0.30%	0.49%	0.05%	0.01%
HT29	98.13%*	0.46%*	1.26%*	0.04%*	0.12%*
TSA	0.27%	0.14%	0.16%	0.01%	0.01%

Table 3
RNA ribose isotopomer distribution of ^{13}C, expressed as % of total ribose, in NCM460 and HT29 cells after TSA treatment. Ct, control cells; TSA, trichostatin-A treated cells. $p < 0.01$ (*) was considered to indicate statistic significant differences between TSA-treated and non-treated cells in each cell line.

RIBOSE	m0	m1	m2	m3	RIBOSE	m0	m1	m2	m3
NCM460	69.69%	18.34%	8.58%	2.46%	HT29	57.65%	27.09%	10.59%	3.86%
Ct	0.29%	0.13%	0.05%	0.05%	Ct	0.29%	0.07%	0.06%	0.10%
NCM460	59.81%*	23.21%*	12.52%*	3.21%*	HT29	65.65%*	19.28%*	11.14%	2.82%*
TSA	0.37%	0.12%	0.14%	0.05%	TSA	0.95%	0.51%	0.32%	0.09%

The second part of our study focused on determining whether a cell differentiation inducer such as TSA [18,19] has the capacity to revert the metabolic phenotype of HT29 cells to that of the non-tumour cells. The metabolic profile accompanying HT29 TSA-induced cell differentiation has recently been reported [8]. It is known that TSA inhibits HDACs and arrests cell cycle at G2/M phase in HT29 cells. These factors lead

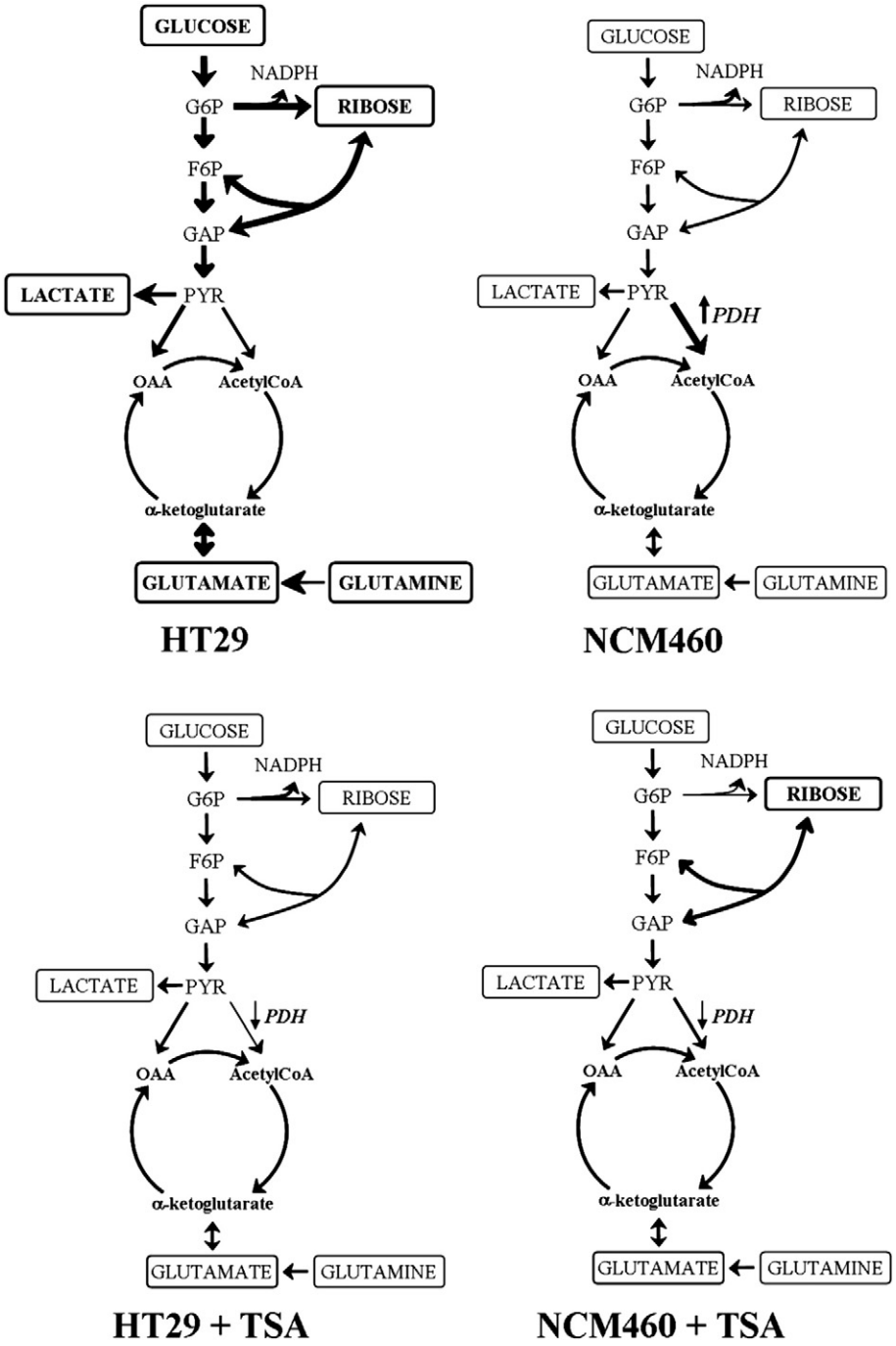

Fig. 3. Diagrams representing HT29 and NCM460 cell metabolism before and after TSA treatment. The main fluxes in the glucose metabolic network are shown. Thicker arrows indicate higher fluxes. G6P, glucose-6-phosphate; GAP, glyceraldehyde-3-phosphate; F6P, fructose-6-phosphate; PYR, pyruvate; OAA, oxalacetate; PDH, pyruvate dehydrogenase; TSA, trichostatin-A.

to the antiproliferative effects of the compound, which in turn is in agreement with the reversion of the phenotype observed. According to [20], cell proliferation requires metabolic sources for the duplication of DNA and cell size, so it is not surprising that the antiproliferative effects of TSA are accompanied by a reduction in ribose enrichment. In the present study, we treated NCM460 and HT29 cells with TSA and compared the results. The results showed that TSA do not alter the metabolism of NCM460 cells. However, the metabolic phenotype of NCM460 cells (TSA-treated or non-treated) was similar to that of TSA-induced HT29 differentiated cells, which is in turn similar to the butyrate-induced HT29 differentiation. This observation suggests that NCM460 cells provide a suitable model of non-tumour cell line for use in comparative metabolic studies and for the analysis of side effects after targeting changes in the tumour metabolic network. Indeed, TSA treatment in HT29 cells reduced glutamine uptake and the glycolytic rate to the same levels as in NCM460 cells. Nevertheless, TSA treatment decreased total ^{13}C glutamate enrichment in the media of both cell lines. This result is not surprising given that, in addition to inducing cell differentiation, TSA triggers the expression of pyruvate dehydrogenase kinase-4 (*PDK4*) [21]. PDK, in turn, inhibits pyruvate dehydrogenase (PDH), thereby preventing pyruvate entry into the Krebs cycle.

Regarding pentose phosphate synthesis, TSA minimally altered the ox/non-ox ratio in NCM460 cells but induced a significant increase in total ribose enrichment ($\sum$ mn), thus indicating an increased PPP flux. This result can also be explained because TSA decreases the entrance of pyruvate into the TCA cycle by increasing *PDK4* expression and this can lead to the accumulation of glycolytic intermediates, which can then be redirected to the PPP. Interestingly, TSA treatment in HT29 cells reduces total ^{13}C ribose enrichment and the ox/non-ox ratio to values similar to those obtained in non-treated NCM460 cells. This action could be linked to the differentiation process since it decreases the need of pentose synthesis for nucleotide production, associated with high proliferation rates, thus counteracting the possible increase in PPP flux caused by PDH inhibition.

5. Conclusions

Our results demonstrate that the NCM460 cell line exhibits a characteristic non-tumour metabolic profile. Therefore, their characteristics make them suitable for comparative purposes in metabolic studies of tumour cells. Furthermore, the observation that the NCM460 line maintains its metabolic homeostasis in response to external perturbations (such as TSA treatment), while the tumour counterpart HT29 shows dramatic changes at metabolic level, proves that the robustness of the tumour metabolome is accompanied by weaknesses to external perturbations that are the Achilles' heel of cancer cell homeostasis. Greater understanding of the metabolic differences between tumour and non-tumour cells opens up avenues for the design of new therapies that specifically target the metabolic adaptation of cancer cells. Moreover, taking into account that nowadays there are some HDAC inhibitors in clinical trials [22–25], our results reinforce the idea of the reversion of metabolic reprogramming to normal colon cells as a crucial mediator of differentiation induced by HDAC inhibitors, and that the use of this class of compounds could ultimately help in cancer therapeutics.

Acknowledgments

The authors thank Ms. Ursula Valls for technical assistance in the experiments. We are also grateful to Robin Rycroft of the Language Services of the Universitat de Barcelona for valuable assistance in the preparation of the manuscript. Financial support was provided by Spanish Government (SAF2011-25726 and personal financial support-FPU program); Spanish Networks RTICC (RD06/0020/004, RD06/0020/1019); AGAUR-Generalitat de Catalunya (2009SGR1308, Icrea Academia award 2010 to M.C.); European Commission (FP7) (ETHERPATHS KBBE-grant agreement 222639, COSMOS KBBE-grant agreement 312941).

References

[1] O. Warburg, On the origin of cancer cells, Science (New York, N.Y.) 123 (1956) 309–314.
[2] C. Munoz-Pinedo, N. El Mjiyad, J.E. Ricci, Cancer metabolism: current perspectives and future directions, Cell Death Dis. 3 (2012) e248.
[3] A. Schulze, A.L. Harris, How cancer metabolism is tuned for proliferation and vulnerable to disruption, Nature 491 (2012) 364–373.
[4] S. Sanchez-Tena, G. Alcarraz-Vizan, S. Marin, J.L. Torres, M. Cascante, Epicatechin gallate impairs colon cancer cell metabolic productivity, J. Agric. Food Chem. 61 (2013) 4310–4317.
[5] E. Im, J. Jung, S.H. Rhee, Toll-like receptor 5 engagement induces interleukin-17C expression in intestinal epithelial cells, J. Interferon Cytokine Res. 32 (2012) 583–591.
[6] B.R. You, W.H. Park, Trichostatin A induces apoptotic cell death of HeLa cells in a Bcl-2 and oxidative stress-dependent manner, Int. J. Oncol. 42 (2013) 359–366.
[7] M.P. Moyer, L.A. Manzano, R.L. Merriman, J.S. Stauffer, L.R. Tanzer, NCM460, a normal human colon mucosal epithelial cell line, In Vitro Cell. Dev. Biol. 32 (1996) 315–317.
[8] G. Alcarraz-Vizan, J. Boren, W.N. Lee, M. Cascante, Histone deacetylase inhibition results in a common metabolic profile associated with HT29 differentiation, Metabolomics 6 (2010) 229–237.
[9] W.N. Lee, L.G. Boros, J. Puigjaner, S. Bassilian, S. Lim, M. Cascante, Mass isotopomer study of the nonoxidative pathways of the pentose cycle with [1,2-13C2]glucose, Am. J. Physiol. 274 (1998) E843–E851.
[10] J. Boren, W.N. Lee, S. Bassilian, J.J. Centelles, S. Lim, S. Ahmed, L.G. Boros, M. Cascante, The stable isotope-based dynamic metabolic profile of butyrate-induced HT29 cell differentiation, J. Biol. Chem. 278 (2003) 28395–28402.
[11] J.M. Lee, E.P. Gianchandani, J.A. Papin, Flux balance analysis in the era of metabolomics, Brief. Bioinform. 7 (2006) 140–150.
[12] P. Vizan, L.G. Boros, A. Figueras, G. Capella, R. Mangues, S. Bassilian, S. Lim, W.N. Lee, M. Cascante, K-ras codon-specific mutations produce distinctive metabolic phenotypes in NIH3T3 mice [corrected] fibroblasts, Cancer Res. 65 (2005) 5512–5515.
[13] C.V. Dang, MYC on the path to cancer, Cell 149 (2012) 22–35.
[14] J.P. Bayley, P. Devilee, The Warburg effect in 2012, Curr. Opin. Oncol. 24 (2012) 62–67.
[15] L.G. Boros, P.W.N. Lee, J.L. Brandes, M. Cascante, P. Muscarella, W.J. Schirmer, W.S. Melvin, E.C. Ellison, Nonoxidative pentose phosphate pathways and their direct role in ribose synthesis in tumors: is cancer a disease of cellular glucose metabolism? Med. Hypotheses 50 (1998) 55–59.
[16] A. Ramos-Montoya, W.N. Lee, S. Bassilian, S. Lim, R.V. Trebukhina, M.V. Kazhyna, C.J. Ciudad, V. Noe, J.J. Centelles, M. Cascante, Pentose phosphate cycle oxidative and nonoxidative balance: a new vulnerable target for overcoming drug resistance in cancer, Int. J. Cancer 119 (2006) 2733–2741.
[17] M. Zanuy, A. Ramos-Montoya, O. Villacanas, N. Canela, A. Miranda, E. Aguilar, N. Agell, O. Bachs, J. Rubio-Martinez, M.D. Pujol, W.N. Lee, S. Marin, M. Cascante, Cyclin-dependent kinases 4 and 6 control tumor progression and direct glucose oxidation in the pentose cycle, Metabolomics 8 (2012) 454–464.
[18] H.F. Duncan, A.J. Smith, G.J. Fleming, P.R. Cooper, Histone deacetylase inhibitors induced differentiation and accelerated mineralization of pulp-derived cells, J. Endod. 38 (2012) 339–345.
[19] X. Hu, X. Zhang, L. Dai, J. Zhu, Z. Jia, W. Wang, C. Zhou, Y. Ao, Histone deacetylase inhibitor trichostatin A promotes the osteogenic differentiation of rat adipose-derived stem cells by altering the epigenetic modifications on runx2 promoter in a BMP signaling-dependent manner, Stem Cells Dev. 22 (2013) 248–255.
[20] P. Vizan, G. Alcarraz-Vizan, S. Diaz-Moralli, O.N. Solovjeva, W.M. Frederiks, M. Cascante, Modulation of pentose phosphate pathway during cell cycle progression in human colon adenocarcinoma cell line HT29, Int. J. Cancer 124 (2009) 2789–2796.
[21] H.S. Kwon, B. Huang, N. Ho Jeoung, P. Wu, C.N. Steussy, R.A. Harris, Retinoic acids and trichostatin A (TSA), a histone deacetylase inhibitor, induce human pyruvate dehydrogenase kinase 4 (PDK4) gene expression, Biochim. Biophys. Acta 1759 (2006) 141–151.
[22] A. Grabarska, M. Dmoszynska-Graniczka, E. Nowosadzka, A. Stepulak, Histone deacetylase inhibitors - molecular mechanisms of actions and clinical applications, Postepy Hig. Med. Dosw. (Online) 67 (2013) 722–735.
[23] S.P. Perrine, O. Hermine, T. Small, F. Suarez, R. O'Reilly, F. Boulad, J. Fingeroth, M. Askin, A. Levy, S.J. Mentzer, M. Di Nicola, A.M. Gianni, C. Klein, S. Horwitz, D.V. Faller, A phase 1/2 trial of arginine butyrate and ganciclovir in patients with Epstein-Barr virus-associated lymphoid malignancies, Blood 109 (2007) 2571–2578.
[24] B.W. Shi, W.F. Xu, The development and potential clinical utility of biomarkers for HDAC inhibitors, Drug Discov. Ther. 7 (2013) 129–136.
[25] A. Villar-Garea, M. Esteller, Histone deacetylase inhibitors: understanding a new wave of anticancer agents, Int. J. Cancer 112 (2004) 171–178.